Thermal deformation and stress of alkali-activated slag concrete under semi-adiabatic condition

Experiments and simulations

Li, Zhenming; Liang, Xuhui; Liu, Chen; Liang, Minfei; van Breugel, Klaas; Ye, Guang

DOI
10.1016/j.cemconres.2022.106887

Publication date
2022

Document Version
Final published version

Published in
Cement and Concrete Research

Citation (APA)
Li, Z., Liang, X., Liu, C., Liang, M., van Breugel, K., & Ye, G. (2022). Thermal deformation and stress of alkali-activated slag concrete under semi-adiabatic condition: Experiments and simulations. *Cement and Concrete Research*, *159*, Article 106887. https://doi.org/10.1016/j.cemconres.2022.106887

Cement and Concrete Research 159 (2022) 106887

Contents lists available at ScienceDirect

Cement and Concrete Research

journal homepage: www.elsevier.com/locate/cemconres

Thermal deformation and stress of alkali-activated slag concrete under semi-adiabatic condition: Experiments and simulations

Zhenming Li *, Xuhui Liang, Chen Liu, Minfei Liang, Klaas van Breugel, Guang Ye

Department of Materials and Environment (Microlab), Faculty of Civil Engineering and Geoscience, Delft University of Technology, Delft, the Netherlands

ARTICLE INFO

Keywords:
Thermal deformation
Autogenous deformation
Semi-adiabatic condition
Cracking
Alkali-activated concrete

ABSTRACT

This study investigates the deformation of free and stress of restrained alkali-activated slag concrete (AASC), respectively, under semi-adiabatic condition. The concrete shows first thermal expansion, which is compensated soon by autogenous shrinkage. The subsequent cooling down of the concrete aggravates shrinkage and development of tensile stress, which eventually results in early cracking of the concrete. The results show that semi-adiabatic condition is severer for AASC than isothermal condition in view of cracking tendency. The evolutions of coefficient of thermal expansion (CTE) and elastic modulus are measured by elaborated experimental methods. Simulating the deformation of AASC by summing thermal and autogenous deformations appears feasible. With the consideration of relaxation, the stress evolution in restrained AASC can be predicted pretty well by the model used in this paper. This study provides insights into the thermal deformation and cracking tendency of AASC in practical circumstances.

1. Introduction

Alkali-activated materials (AAMs) and/or geopolymers have emerged as eco-friendly alternatives to ordinary Portland cement (OPC). The main motivations of the industry to use AAMs come from the possibilities to reuse industrial by-products or waste and to reduce CO_2 emissions [1]. Other advantages of AAMs include high strength, superior durability and fire resistance [2–4]. However, the application of alkali-activated concrete (AAC) in construction engineering is still limited. Drawbacks hindering a wide application of AAC include fast setting, large shrinkage, efflorescence, etc. [5–7]. Among these, the large shrinkage is a serious concern since it can induce micro- or macro-cracking of the concrete, while cracking will further impair the durability of infrastructures.

For concrete, there are mainly 6 types of shrinkages: chemical shrinkage, autogenous shrinkage, plastic shrinkage, drying shrinkage, carbonation shrinkage and thermal shrinkage [8]. Among them, chemical shrinkage is an intrinsic behaviour of the binder and develops with on-going chemical reactions. Chemical shrinkage itself is not harmful, but it may go along with self-desiccation and built-up of capillary tension in the pores, which leads to autogenous shrinkage [9]. While plastic shrinkage, drying shrinkage and carbonation shrinkage are triggered by substance exchange with the environment and can be therefore eliminated by avoiding moisture loss and CO_2 ingress, autogenous shrinkage is a spontaneous process that is almost inevitable. In the past decade, increasing research attention has been drawn to the autogenous shrinkage and the consequent cracking risk of AAMs [10–13]. While previous studies made substantial contributions to the understanding of the mechanism and mitigating strategies of autogenous shrinkage of AAMs, it is evident that the deformation of concrete under practical conditions is never strictly autogenous. Thermal deformation is always involved due to the fact that both the environmental temperature and the internal temperature of concrete change with time. A common case is the temperature rise in concrete due to the heat release of exothermic reactions and the subsequent cooling to reach equilibrium with the environment. In other words, concrete in real structure is usually under a semi-adiabatic condition rather than isothermal condition [14]. The restraint of thermal shrinkage, e.g. by reinforcement, ground or adjacent concrete, will cause tensile stress in the concrete and even cracking, especially when combined with autogenous shrinkage [15].

However, literature on thermal deformation of AAC, especially under semi-adiabatic condition, is scarce [16–20]. Part of the reason lies in the complex nature of thermal deformation that couples with reactions and autogenous shrinkage. In fact, the interplay of autogenous shrinkage and thermal deformation during hydration has not been thoroughly understood even for OPC concrete [21]. Besides, due to the

* Corresponding author.
E-mail address: z.li-2@tudelft.nl (Z. Li).

https://doi.org/10.1016/j.cemconres.2022.106887
Received 30 December 2021; Received in revised form 7 April 2022; Accepted 11 June 2022
Available online 18 June 2022

different chemistry and microstructure of OPC and AAMs, the available experimental data on reaction heat and thermal parameters, e.g. coefficient of thermal expansion (CTE), thermal conductivity, specific heat, etc. of OPC cannot be directly applied for AAMs. Other issues to be considered concern creep and relaxation. As reported in [22,23], AAMs based on slag show much more pronounced viscoelasticity than OPC, due to which, simply estimating the stress development in restrained AAC by free deformation and elastic modulus will lead to larger error. In summary, it is not possible to evaluate the thermal deformation and cracking potential of AAC serving under non-isothermal conditions using existing knowledge.

Against this background, this study is conducted to experimentally investigate the deformations and stresses of alkali-activated slag concrete (AASC) under semi-adiabatic condition. The experimental results are compared with those obtained under isothermal conditions and also those on OPC concrete. Through revisited experimental designs, we also measured the evolutions of CTE and elastic modulus, which are important inputs for the simulation. The knowledge on autogenous shrinkage of AASC allows us to separate the thermal deformation from autogenous shrinkage. By considering relaxation, we simulated the stress of restrained AASC.

2. Methodology

2.1. Outline of the study

This study consists of two parts: experimental measurements and simulation, as shown in Fig. 1. Two Autogenous Deformation Testing Machines (ADTMs) and one Temperature Stress Testing Machine (TSTM) were employed to measure the deformation and stress of the concrete in free and restrained condition, respectively. The temperature history in the concrete specimens was monitored by thermocouples. The evolutions of CTE and elastic modulus of the concrete were measured by ADTM and TSTM, respectively, with specially designed temperature or loading strategies. The experimental methods are described in detail in the following section. The deformation of the concrete under semi-adiabatic condition was simulated as the sum of thermal deformation and autogenous deformation. Stress simulation were performed making allowance for the relaxation of the concrete. In this study, simulation means the application of these principles to analytically describe parameters like deformation and stress.

2.2. Raw materials and mixture proportion

The precursor used to produce AASC was ground granulated blast furnace slag (hereinafter termed slag) supplied by Ecocem Benelux BV. X-ray fluorescence (XRF) was used to characterize the chemical compositions of the slag, as shown in Table 1. The density of slag was 2.89 g/cm^3. Alkaline activator was a combination of NaOH pellets (analytically pure), deionized water and Na_2SiO_3 solution. The Na_2SiO_3 solution was supplied by Brenntag, with 27.5 wt% of SiO_2 and 8.25 wt% of Na_2O. Per 100 g of activator contained 13.8 g of SiO_2, 9.4 g of Na_2O and 76.8 g of water (i.e., $M_S = 1.5$). The water-to-solid ratio of the paste was 0.344, if SiO_2 and Na_2O in the activator are considered as parts of solid.

2.3. Experimental approaches

2.3.1. Temperature evolution of AASC under semi-adiabatic condition

The semi-adiabatic condition was realized by the insulation of moulds of ADTM1 (Fig. 2 (a)). The moulds were made of 40 mm-thick foam plastics with a low coefficient of heat conductivity (0.03 J/(s·m·K)), around two-order lower than that of normal weight aggregate concrete. The foam plastic was covered by wood plates. At one side of the parts, canals were cut in the wood plate, where rubber tubes were placed (Fig. 2 (b)). These tubes can be connected to a cryostat to cool or heat the concrete surface by circulating water. A steel plate with thickness of 1 mm was glued to the wood plate to ensure a smooth inner surface of the mould and to cover the canals cut in the wood plate. For ADTM1 which was used to provide semi-adiabatic condition, the tubes were empty, while the ones in ADTM2 and TSTM were connected with cryostats. The whole set-up was placed in a temperature-controlled chamber, whose temperature was kept between 19.2 and 19.5 °C.

The temperature of concrete was measured by thermocouples located in the centre of the concrete specimen. In the ADTMs specimens, three thermocouples were placed, one in the middle and two near the positions of the measuring bars where LVDTs were connected. The temperature along the length of the concrete specimens was found homogenous with the temperature difference among the three positions smaller than 0.1 °C. Therefore, only the temperature of the middle thermocouple is shown. As the thermocouples were inserted during casting, temperature measurement and control can start immediately after casting. The temperature was recorded every minute.

2.3.2. Free deformation of AASC under semi-adiabatic condition

The free deformation of AASC under semi-adiabatic condition was measured by ADTM1. The ADTM covered all the surfaces of the concrete prism (1000 × 150 × 100 mm^3) with four LVDTs connected to measure the length change of the concrete. The LVDTs had a measuring resolution of 1 μm. The LVDTs measured the movement of the steel bars which were embedded in the concrete during casting and passed through small holes in the mould. The distance between the two cast-in steel bars was 750 mm. Detailed information on connection of the LVDTs with measuring bars can be found in [24]. The LVDTs were installed at 6 h after casting, when the concrete obtained a certain stiffness. In fact, the concrete lost its workability at 35 min after casting, but its stiffness was reported to be low in the first hours (see Appendix A). Therefore, the

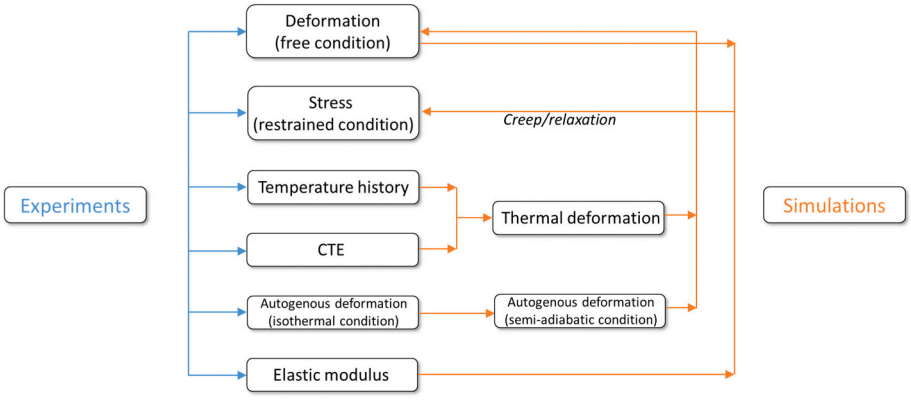

Fig. 1. Outline of this study.

Table 1
Chemical compositions of slag.

Precursor	Component (mass% as oxide)								
	SiO_2	Al_2O_3	CaO	MgO	Fe_2O_3	SO_3	K_2O	TiO_2	Other
Slag	31.8	13.3	40.5	9.3	0.5	1.5	0.3	1.0	1.9

Quartz river sand (0–4 mm) and round gravels (4–8 mm and 8–16 mm) were used as aggregates. The mixture proportion of AASC is shown in Table 2.

Table 2
Mixture proportion of AASC.

Components (kg/m^3)	AAS
Slag	400
Activator	200
Aggregate [0–4 mm]	789
Aggregate [4–8 mm]	440
Aggregate [8–16 mm]	525
Volume fraction of aggregate	0.67

measurement was not started immediately after casting to ensure stable positioning of the measuring bars. The deformation was recorded every minute from 6 h to 28d.

2.3.3. Stress of restrained AASC under semi-adiabatic condition

The stress in a restrained AASC specimen was measured with the TSTM, as shown in Fig. 3. The specimen had a dog-bone shape and the testing area of interest was prismatic with the same size as the specimen in ADTMs, i.e. 1000 × 150 × 100 mm^3. The prismatic part of the machine was equipped with the same type of moulds and LVDTs as the ADTMs. Detailed description of the TSTM can be found in [25]. The load was recorded with the load-cell with a loading capacity of 100 kN and a resolution of 0.05 kN. The specimens in ADTMs and TSTM were cast from the same batch of concrete to ensure the same material behaviour. The temperature of concrete in TSTM was controlled the same as in ADTM1. The measurement of the stress started at 6 h. The stress was recorded every minute until 28d.

During testing, the deformation of the middle prismatic part was kept at zero (nominally, in reality within ±1 μm). The length of the whole specimen may not be constant since the steel claws gripping the concrete heads had higher thermal conductivity than the foam mould in the middle. During reaction, the head parts of the concrete experienced slightly different temperature evolutions, thus different thermal deformations, from the middle part. The temperature within the prismatic part of interest was basically homogenous.

A sudden decrease in the stress to around zero indicated the occurrence of cracking of the concrete. Two replicate tests were conducted. The maximum stresses detected in the two tests showed a difference as small as 3 %. Cracking of the concrete was observed after 1.4d and 1.37d, respectively, with a difference of only 40 min. This indicates a good repeatability of the test. In Section 3, therefore, only the results from one test will be shown.

2.3.4. CTE of AASC under semi-adiabatic condition

2.3.4.1. Temperature regime. The CTE of the concrete was measured by ADTM2. In most of the time, the temperature of concrete in ADTM2 ($T2$) was kept the same as that in ADTM1 ($T1$). At certain ages, however, the temperature of concrete in ADTM2 was manually changed to $T1 + 1$ or $T1 - 1$ and then back to $T1$ when the change was done. The corresponding deformation during the temperature change was recorded to obtain the CTE. This kind of temperature cycles was applied three times (6 h, 12 h, 24 h) in the first day and every day afterwards till 28d. Each cycle took around 2 h. Since increasing or decreasing the temperature even by 1 °C could slightly influence the reaction degree of the concrete, $T1+$ 1 °C and $T1-$ 1 °C were set alternatively as the target temperature ($T2_T$) in the period of 28d, to minimize the influence of temperature history on the maturity of concrete.

To ensure a fast switch from $T2$ to any $T2_T$, the temperature of circulating water ($T2_S$) in the mould was set with a difference 10 times larger, as shown in Eq. (1). A cryostat received orders from the computer and controlled the temperature of circulating water ($T2_W$). It is noted that $T2_W$ was not always equal to $T2_S$ especially when a sudden change was given to $T2_S$ since heating or cooling of water needs a bit of time.

$$(T2_S - T2) = 10 \times (T2_T - T2) \quad (1)$$

An example of the temperature change in the concrete is shown in

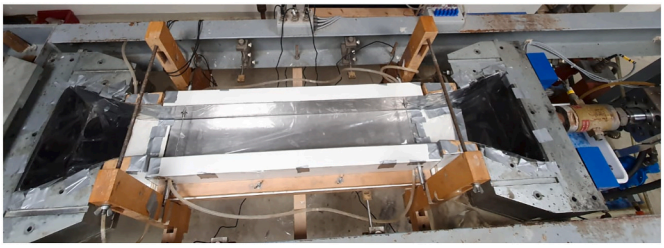

Fig. 3. The TSTM used for stress measurement. The top mould will be installed after concrete casting.

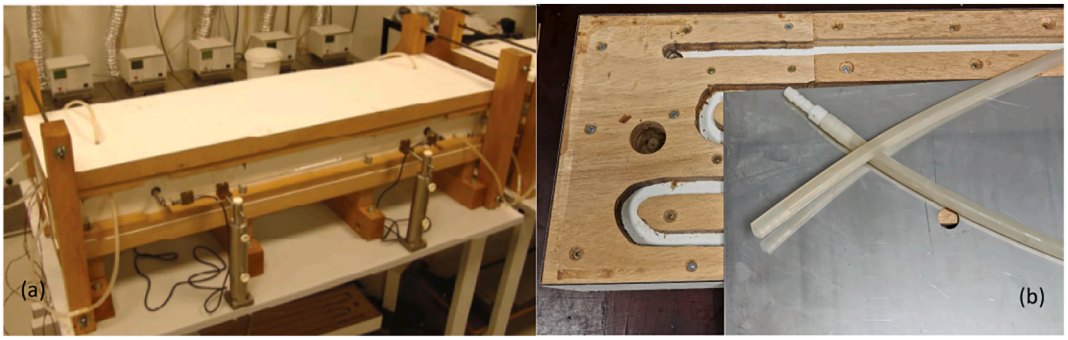

Fig. 2. (a) An ADTM used for deformation measurement. (b) Configuration of the mould, made by foam, wood, rubber tube and steel plate. Canals were cut in the inner surface of the mould.

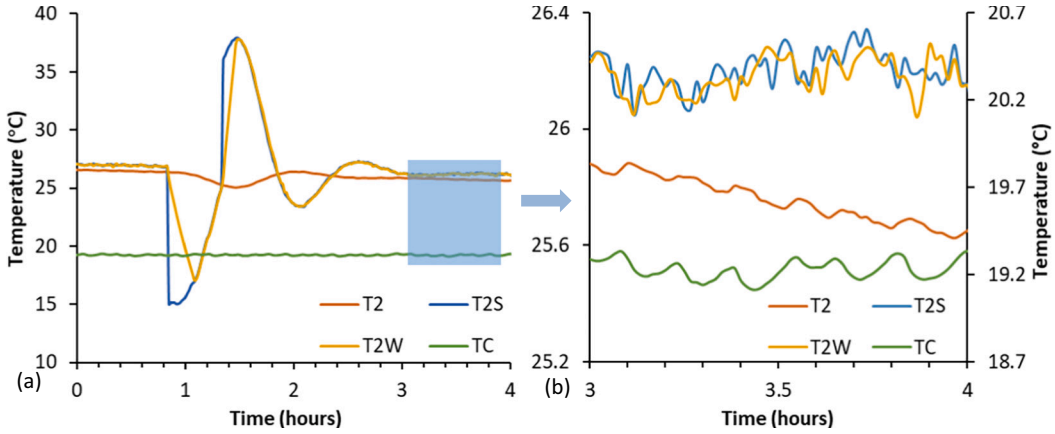

Fig. 4. (a) Temperature reduction in the concrete in ADTM2 by 1 °C at the age of 34 h. The temperature was set back after reaching the target. $T2$, $T2_S$, $T2_W$, and T_C denotes temperature of the concrete, set temperature and temperature of the circulating water, and temperature of the chamber, respectively. A zoomed region is shown in (b), where T_C is shown on the secondary axis.

Fig. 4 (a). Initially, $T2_W$ was slightly higher than $T2$ to compensate the heat loss to the environment. Then a temperature reduction of 1 °C was applied on the concrete. To quickly cool down the concrete, $T2_S$ was set around 10 °C lower (see Eq. (1)) and $T2_S$ went down correspondingly. Since the concrete had a certain thickness (150 × 100 mm^2), the cooling of concrete took a bit of time, therefore $T2$ did not decrease immediately after $T2_W$ but lagged behind for several minutes.

As $T2$ gradually decreased, $T2_S$ and $T2_W$ increased due to the smaller difference between $T2$ and $T1 - 1$. At the moment when $T2$ reached $T1 - 1$ °C, $T2_T$ was set back to $T1$, hence $T2_S$ was set around 10 °C higher to heat up the concrete. Because of the lagging temperature change in the concrete, the actual reduction in $T2$ was larger than 1 °C. For the same reason, it always took more than one cool down-and-heat up cycle before $T2$ stabilized at $T1$, only the amplitude of each temperature cycle became lower and lower.

It is also noticed that temperature curves of the concrete were not smooth. As zoomed in Fig. 4 (b), the temperature evolutions were actually composed of many small waves with the amplitude of around 0.05 °C. This was because the temperature of the chamber T_C was not strictly constant. Rather, it fluctuated by around 0.2 °C all the time. $T2_W$ hence underwent cyclic adjustments aiming to compensate the small fluctuation in ambient temperature and correspondingly, $T2$ fluctuated slightly too.

2.3.4.2. Calculation of CTE. The concrete deformation corresponding to the temperature change shown in Fig. 4 is presented in Fig. 5. As marked by the dashed lines, the changes in $T2$ lagged a little behind the deformation. This is because the deformation was dependent on the overall or average temperature of the concrete while $T2$ was the temperature of the centre part of concrete, which changed a bit later than that of the concrete surface. Associated with the temperature fluctuations, the deformation curve also shows small fluctuations. These fluctuations lead to difficulty in determining the ending moment of each thermal cycle when the changing amplitude is low. Hence, only the first cycle consisting of significant shrinkage and expansion, as marked in between the dashed lines, is used to calculate CTE. The starting times of $\Delta\varepsilon_1$ and ΔT_1 were defined as the moment when their curves reached the last peak/trough (slope equals to 0) during fluctuation before the slope of the curves change dramatically.

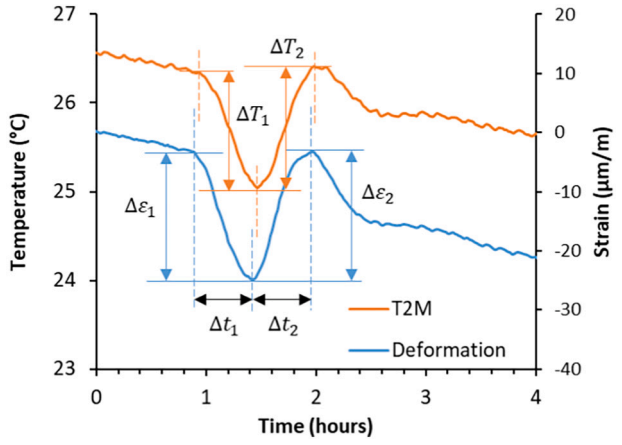

Fig. 5. Deformation of the concrete associated with temperature change at the age of 34 h.

It should be noted that, however, the measured $\Delta\varepsilon_1$ and $\Delta\varepsilon_2$ were not strictly thermal deformation. Autogenous shrinkage also contributed even though the time intervals (Δt_1 and Δt_2) were short. To obtain the CTE, autogenous shrinkage should be separated from the thermal deformation, as shown in Eq. (2).

$$\alpha_{CTE} = \frac{\Delta\varepsilon_{th}}{\Delta T} = \left(\frac{\Delta\varepsilon_{th1}}{\Delta T_1} + \frac{\Delta\varepsilon_{th2}}{\Delta T_2}\right)\Big/2 = \left(\frac{\Delta\varepsilon_1 - \Delta\varepsilon_{au1}}{\Delta T_1} + \frac{\Delta\varepsilon_2 + \Delta\varepsilon_{au2}}{\Delta T_2}\right)\Big/2$$
$$= \left(\frac{\Delta\varepsilon_1}{\Delta T_1} + \frac{\Delta\varepsilon_2}{\Delta T_2}\right)\Big/2 + \left(\frac{\Delta\varepsilon_{au1}}{\Delta T_1} - \frac{\Delta\varepsilon_{au2}}{\Delta T_2}\right)\Big/2 \quad (2)$$

where $\Delta\varepsilon_{th}$ and $\Delta\varepsilon_{au}$ is the thermal strain and autogenous shrinkage in a certain time interval, respectively. ΔT is the temperature difference. $\Delta\varepsilon_1$ and $\Delta\varepsilon_2$ are the successive deformations during the first temperature cycle, as shown in Fig. 5.

Since the time intervals Δt_1 and Δt_2 were short (around 0.5 h), the developing rate of autogenous shrinkage in this period can be assumed as constant. Since the same function was used to cool down and to heat up the water circulating around the concrete (Eq. (1)), the increasing and decreasing rates of the concrete temperature were rather similar. Therefore, the sum of the terms for autogenous shrinkage in Eq. (2) is approximately equal to zero, as derived in Eq. (3).

$$\frac{\Delta\varepsilon_{au1}}{\Delta T_1} - \frac{\Delta\varepsilon_{au2}}{\Delta T_2} = \frac{r \bullet \Delta t_1}{\Delta T_1} - \frac{r \bullet \Delta t_1}{\Delta T_2} = r \bullet \left(\frac{\Delta t_1}{\Delta T_1} - \frac{\Delta t_1}{\Delta T_2}\right) \approx 0 \quad (3)$$

where r is the developing rate of autogenous shrinkage in the time intervals Δt_1 and Δt_2.

In this case, the CTE of the concrete can be approximately calculated as Eq. (4).

$$\alpha_{CTE} = \left(\frac{\Delta\varepsilon_1}{\Delta T_1} + \frac{\Delta\varepsilon_2}{\Delta T_2}\right) \Big/ 2 \quad (4)$$

2.3.4.3. Additional remarks on CTE measurement. Two remarks need to be added here on the method proposed in this section. First, the early-age deformation of concrete is associated with continuous reaction, the kinetics of which is critically influenced by the curing temperature. Hence, it is vital to minimize the temperature shock when measuring the CTE, in view of not only the magnitude but also duration. That is the reason why the temperature of the concrete was changed by only 1 °C and set back immediately after the target was reached. For the same reason, the adjusting factor of 10 was chosen (see Eq. (1)) to ensure a fast heating or cooling of the concrete for 1 °C.

One may argue that 1 °C might be not enough to generate a detectable deformation of the concrete. For example, thermal pulses of plus and minus 5 °C were used in [38] to determine the CTE. However, as shown in Fig. 5, the deformation was large enough to be detected by the machine given a relatively small fluctuation in the chamber temperature. Besides, trail tests were conducted changing the concrete temperature more significantly by, for example, 2 °C or 3 °C after the concrete was mature enough and the calculated CTE was similar. This indicates that the temperature change by only 1 °C is proper to use to obtain the CTE as long as high measuring accuracy of the concrete deformation can be ensured.

The second thing to be noted is that the deformation of concrete due to temperature change may not occur instantaneously. Since concrete (based on either AAS or OPC) is a heterogeneous material, the thermal properties including CET, thermal capacity and thermal conductivity are not the same for unreacted precursors, pore solution, solid products and aggregates. Therefore, time is always needed to reach a temperature equilibrium within the concrete, especially considering that aggregate does not generate heat and needs time to be warmed up. Moreover, AAS is more viscous than OPC [22,23]. The deformation of AAS matrix under external or internal forces, e.g., restraint by aggregates, is actually time-dependent. Therefore, the thermal deformation of AASC should also be time-dependent and may not be accurately obtained in a short period as shown in Fig. 5. However, it is very complex, if not impossible, to separate the instantaneous and time-dependent thermal deformation of concrete, especially in early age when fast reaction is ongoing. Therefore, we have to assume the thermal deformation is elastic and instantaneous here in order to obtain the CTE.

2.3.5. Elastic modulus of AASC under semi-adiabatic condition

The same concrete mixture was cast into TSTM and cured in the same semi-adiabatic condition. To measure the elastic modulus, the machine was set under force control. In the first 6 h, no force or deformation was applied on the sample to avoid immature failure. From 6 h, a compressive force was imposed on the concrete instantly (nominally, in reality from 0.5 s to 1 s depending on the load). The force was designed to generate a stress of around 15 % of the compressive strength estimated based on the strength of AASC cured under isothermal condition [25]. For the concrete cured under semi-adiabatic condition, the strength should be a bit higher and therefore the stress-to-compressive strength ratio would be a bit lower than 15 %. The stress magnitude of around 15 % was chosen with the following consideration. On one hand, the load cannot be too high in case of damage or non-elastic deformation of concrete. Normal concrete is considered in elastic regime under a stress smaller than 15 % of the compressive strength [26]. Within this range, a larger load is preferable to ensure a measurable linear deformation.

After a short period of stabilization at the target load, the concrete was unloaded to 0.3 kN in compression at a rate of 1kN/s, which corresponds to 0.067 MPa/s. The uploading rate was chosen according to [27]. An instant uploading was not chosen to avoid accelerated release of oil in the pump which can cause shifting of the piston in the loading cell. After unloading, the force on the concrete was kept at −0.3kN, rather than 0kN, to keep a slight compression status of the setup. Otherwise, the force could shift between tension and compression and disturb the measurement. A permanent force as small as −0.3kN was believed not to cause damage or apparent creep of the concrete in TSTM.

The loading-uploading cycle was applied every 2 h in the first 14 h of curing and the testing frequency was gradually reduced with the elapse of time. During loading and unloading, the force and deformation data were recorded every 0.1 s to capture the signal frequently. In the rest of the time, the data were recorded every minute. Based on the stress and strain results, elastic modulus can be calculated.

An example of the loading and unloading and corresponding strains is presented in Fig. 6. It can be seen that the loading took around 0.6 s from −0.3kN to −3kN. In later age when the concrete showed higher strength, larger load was applied, but the time used to reach the maximum load was also within 1 s. This ensured a fast loading with minimized development of creep. It can be seen from Fig. 6 that the change in deformation was around 0.3 s behind that in force during both loading and unloading stages. This is plausible since the force needed to move the steel claw before pressing the concrete. After loading or unloading, the length of concrete did not stay constant like the stress. This might be due to creep or creep recovery of the material, which does not belong to elastic deformation. Hence, only the regions marked by the arrows are used for the calculation of elastic modulus, as shown in Eq. (5). The starting time of $\Delta\sigma$ or $\Delta\varepsilon$ are defined as the moments when their increment/decrease starts to exceed 0.1 kN (0.0067 MPa) or 1 μm/m per 0.1 s in two successive time steps. The ending time, correspondingly, is the moment when the change becomes smaller than the threshold in two successive time steps. The reason for the requirement on two successive time steps is to avoid mistaking the fluctuation of 1 data point for signal of stabilization.where $\Delta\sigma$ is the stress change, which is force change (Δf) divided by the cross-section area, at the curing age t. $\Delta\varepsilon$ is the strain change. W is the width (150 mm) and D is the depth (100 mm) of the concrete.

Since both loading and unloading were quick, the concrete can be considered under semi-free condition in most of the time. The elastic moduli obtained using data from loading and uploading stages will be shown and compared in Section 3.

3. Experimental results and discussion

3.1. Temperature evolution of AASC under semi-adiabatic condition

To clearly show the temperature evolution of the concrete in different ages, regions within 4 h, 48 h and 28d of curing are shown individually in Fig. 7 (a)–(c). Fig. 7 (a) shows that the temperature fluctuated from 18 °C to 20 °C during concrete casting. At that time the thermocouples had not been inserted in the concrete and were therefore measuring the air temperature around the facility. After the thermocouples were inserted into the concrete, the readings of the thermocouples became much more stable. The fresh concrete was a bit warmer (20.5 °C) than the environment (19.5 °C) due to mixing and initial reaction heat.

The temperature of the concrete increased from 20.5 °C to around 23 °C in the first hours, as shown in Fig. 7 (a). This is due to the dissolution of the precursors and initial formation of products, like what had been observed by calorimetry on AAS pastes [23]. After 6 h, the temperature of the concrete experienced another surge, as marked by the dashed lines in Fig. 7 (b). While 0–6 h can be considered as the dormant period of the concrete, 6-18 h belongs to the acceleration period in this condition. This verifies the reasonability to start measurements of deformation and stress at 6 h (see Sections 2.3.2 and 2.3.3). As reported in [25], the AASC cured under isothermal condition at 20 °C shows a dormant period of around 8 h and an acceleration period of around 6 h. The comparison with the results here shows that curing at a higher temperature shortens the dormant period and prolongs the acceleration

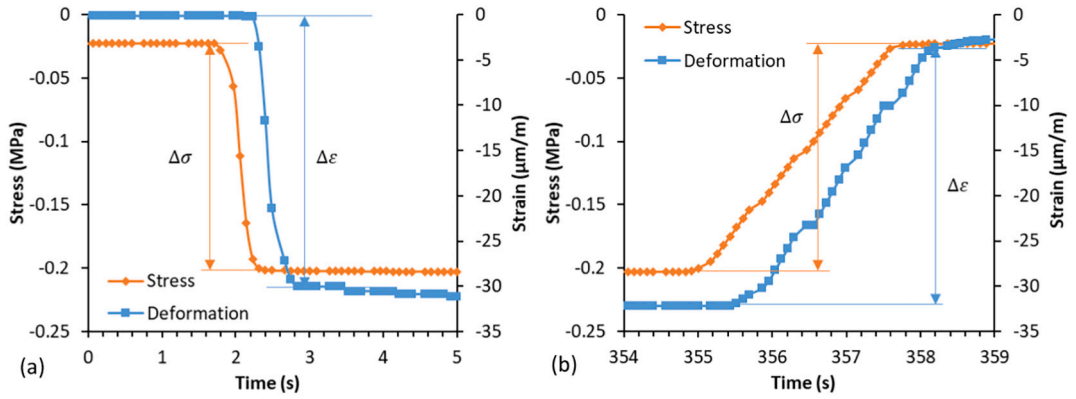

Fig. 6. Loading (a) and unloading (b) of the concrete at the age of around 10 h and corresponding deformations. The starting point of the deformation was set as zero for the convenience of observation.

$$E(t) = \frac{\Delta\sigma(t)}{\Delta\varepsilon(t)} = \frac{\Delta f(t)}{W \bullet D \bullet \Delta\varepsilon(t)} \tag{5}$$

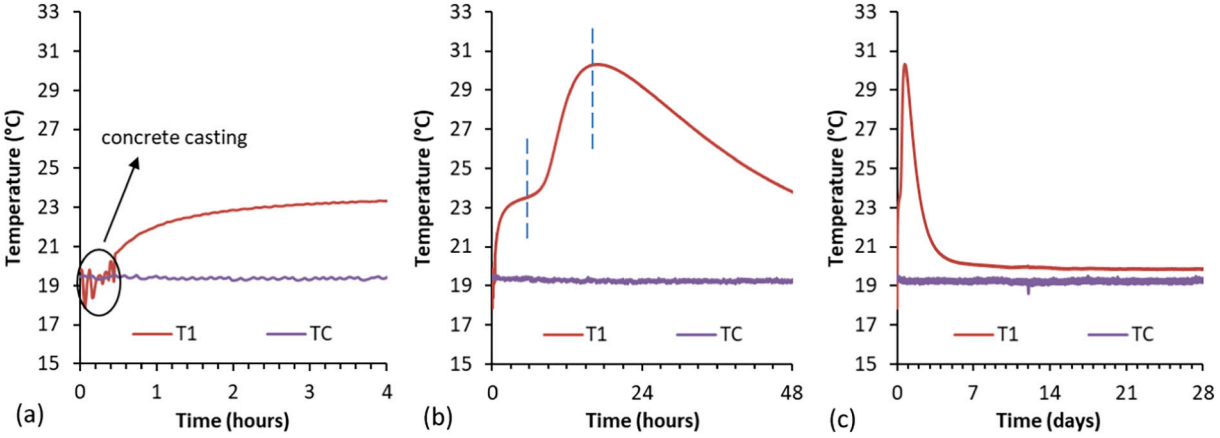

Fig. 7. Temperature evolution of AASC in ADTM1 in 4 h (a), 48 h (b) and 28d (c).

period of AASC.

The temperature of the concrete decreased gradually from 18 h to 7d and plateaued afterwards, as shown in Fig. 7 (c). The stabilized temperature does not mean the stop of reaction, since $T1$ remained higher than T_C till 28d. Rather, it indicates an equilibrium between the heat production and dissipation.

In a previous study [24], Lokhorst measured the temperature history of OPC concrete (water/cement ratio of 0.5, cement content of 350 kg/m^3) under semi-adiabatic condition by the same ADTM. The temperature evolution curves of AASC and OPC concrete are plotted in Fig. 8. It appears that the AASC generated higher reaction heat than OPC concrete in the beginning of casting, which was probably contributed by the fast dissolution of slag in alkaline solution. This is in line with the high initial reaction heat measured by calorimeter on AAS pastes [28]. After the first 6 h, the hydration heat of OPC concrete became much higher than that of AASC, even though the AASC had a higher binder content (400 kg/m^3). The temperature of OPC concrete reached as high as 39 °C within 1d, while the peaking temperature in AASC was only 30 °C. This is consistent with the findings from [11,29] that the formation of C-A-S-H types gels normally generates less heat than cement hydration.

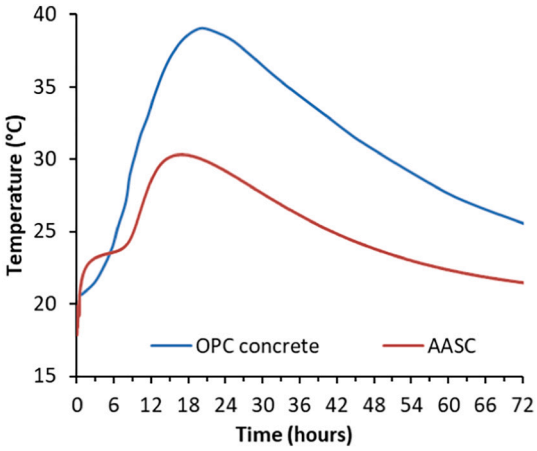

Fig. 8. Temperature evolutions of AASC (l/b = 0.5, binder content 400 kg/m^3) and OPC concrete (w/c = 0.5, binder content 350 kg/m^3) measured by the same ADTM.

3.2. Free deformation of AASC under semi-adiabatic condition

The free deformation of AASC under semi-adiabatic condition is shown in Fig. 9 (a). The figure shows that the deformation curves are smooth with little noise. The LVDTs in the two sides (front and back) of the concrete gave very close results. After 12d, the curves of $D1_F$ and $D1_B$

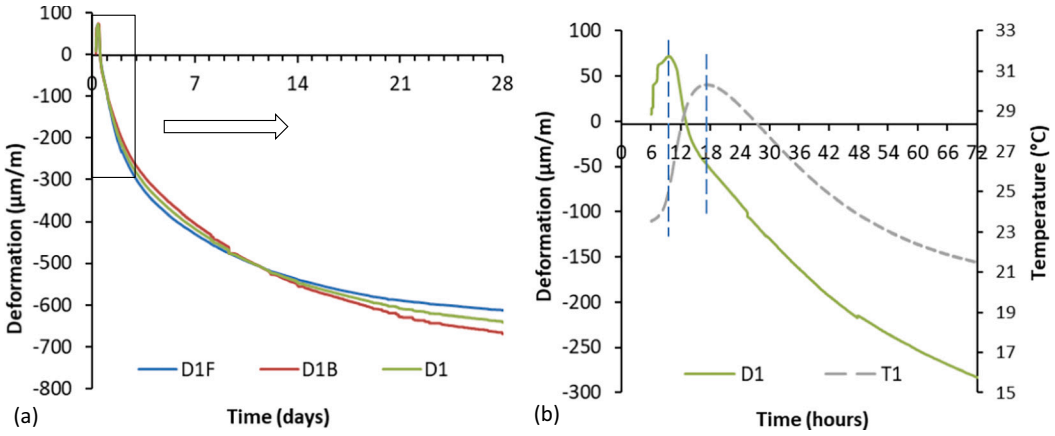

Fig. 9. Free deformation of AASC under semi-adiabatic condition (a). $D1_F$ and $D1_B$ denotes the deformation measured on the front and back side of the concrete, respectively. The region in the first 72 h is zoomed in (b), where T1 (dashed line) is plotted on the secondary axis.

started to diverge, but the discrepancy was only 8 % at 28d. These indicate a well-aligned axial deformation of the concrete and high accuracy of the measurement. It can be seen from Fig. 10 (a) that the concrete first expanded then shrank. The shrinkage was rapid in the first days and kept developing, reaching 640 μm/m at 28d.

The free deformation in the first 72 h is zoomed in Fig. 10 (b), plotted together with the temperature evolution (*T*1, dashed line). The figure shows that the expansion of the concrete was associated with the initial temperature increase from 6 to 9 h. As discussed in Section 3.1, this period was the beginning of the acceleration period of the reaction. From 9 h, the temperature increased rapidly at a rate of >1 °C/h, while the concrete started to shrink rather than to continue the expansion. This phenomenon is interesting and was also identified for some high strength OPC concrete, although OPC systems normally expands at this rate of temperature increment [24,30]. The shrinkage of AASC from 9 to 18 h was attributed to the large autogenous shrinkage in this period [31]. As reported in [32], the autogenous shrinkage of AAS cured under isothermal condition highly correlates to the reaction rate and develops intensively in acceleration period. When the concrete was cured under semi-adiabatic condition, the reaction was self-enhanced due to the temperature rise so that the autogenous shrinkage was also enhanced, thus it compensated the possible thermal expansion. This result indicates the twofold effects of temperature rise: on one hand it can induce thermal expansion, while on the other hand, it can enhance the autogenous shrinkage. The final deformation depends on the competition between these two deformations.

From 18 h, the concrete continued to shrink. The shrinkage was contributed by not only autogenous shrinkage but also thermal shrinkage due to the temperature decrease. After 7d when the temperature already stabilized (see Fig. 7 (c)), the shrinkage of the concrete was mainly contributed by the autogenous shrinkage. This result shows the important role of autogenous shrinkage of AASC under semi-adiabatic condition, not only in very early age but till 28d.

3.3. Stress of restrained AASC under semi-adiabatic condition

The stress evolution in restrained AASC is shown in Fig. 10 (a). In general, the stress curve is smooth except for some small fluctuations. The stress evolution can be roughly divided into four processes. From 6 to 9 h, the compressive stress generated in the restrained concrete was close to zero although the concrete tended to expand due to the temperature increase (see Fig. 9 (b)). This indicates that the stiffness of the concrete remained low in this stage. From 9 to 12 h, the concrete tended to shrink due to the enhanced autogenous shrinkage, so that tensile stress was generated, although the concrete temperature kept increasing in this period. The stress building-up indicates an increased stiffness of the concrete. From 12 to 15 h, the shrinkage rate of the concrete reduced and so it was with the stress. After 15 h, the temperature of the concrete started to decrease and the thermal shrinkage contributed to a second surge of tensile stress.

At around 40 h, the stress of the concrete dropped to zero, indicating the occurrence of cracking. In comparison, the AASC cured under isothermal condition (20 °C) did not crack until 20d as shown in Fig. 10 (b). The starting time of the stress development was later (as marked by the dashed line), probably due to the slower development of stiffness in this condition. After the acceleration period, the stress in AASC cured

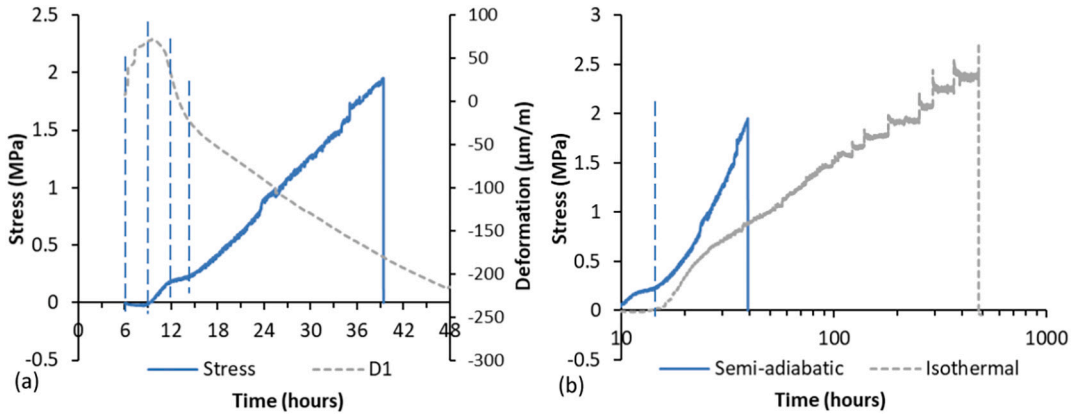

Fig. 10. Stress evolution of restrained AASC plotted together with the free deformation (a). Comparison between the stress evolutions in restrained AASC cured under semi-adiabatic condition and isothermal condition (b). The data for the latter scenario is from [25].

isothermally did not show a second surge thanks to the absence of thermal shrinkage. The higher tensile stress and earlier cracking time of AASC under semi-adiabatic condition show that this condition leads to a higher cracking tendency of AASC than isothermal condition. The cracking time of AASC was also earlier than that of OPC that experienced severer temperature drop (Fig. 8) as reported in [24].

Fig. 11 (a) shows that the cracking occurred on the left side of the beam near the neck area. Some studies suggested that if the CTE of the coarse aggregate and of the paste differ, a large change in temperature may introduce differential movement and a break in the bond between the aggregate particles and the surrounding paste [8]. However, in the scenario studied here, the expansion occurred only before 9 h when the stiffness was low and the shrinkage later on was much higher than the expansion. Hence, debonding between paste and aggregates should not happen. This statement is supported by the feature of the fracture surface of AASC. As shown in Fig. 11 (b), the cracking surface passed not only around but also through the aggregates, indicating a fair bonding between paste and aggregates. Hence, it can be concluded that the early cracking of the concrete cured under semi-adiabatic condition was not attributed to a weakened interfacial transition zone, but the large tensile stress that can break both paste and aggregates.

The results in this section show that semi-adiabatic condition is a severe condition for AASC in view of cracking tendency. For OPC concrete, the temperature increase in the early age normally induces compressive stress [8,33], which is useful to compensate part of the tensile stress during subsequent cooling. However, due to the low stiffness or dramatic viscoelasticity of AASC in the early age, limited compressive stress was generated. Afterwards, the concrete started to shrink due to the enhanced autogenous shrinkage by the elevated temperature. More research attention is definitely needed to find solutions to reduce the tensile stress in AASC cured in semi-adiabatic condition.

3.4. CTE of AASC under semi-adiabatic condition

The CTE evolution of AASC is shown in Fig. 12. This is one of the first times that the evolution of CTE with curing age is obtained for AASC. At the age of 6 h, the CET was rather high. This is consistent with the low stiffness of the young concrete, as will be verified in the next section. Afterwards, the CTE decreased intensively along with the hardening of the concrete, indicated by the increment of stiffness. After 12 h, the CTE of AASC gradually increased with time. This can be explained by the self-desiccation process which leads to a lower internal relative humidity of the concrete [23]. As the relative humidity decreases, the CTE of concrete increases, as reported for OPC systems [34,35]. Despite the fluctuation of the curve, the two-stage evolution of CTE is in line with the results of previous studies on OPC paste or concrete [36–39]. In [21], only an increasing trend of CTE of OPC concrete was observed, but that is probably because the CTE in the first hours was not measured. Comparing the results in literature [21,40–42], it can be seen that AASC shows higher CTE than OPC systems, the CTE of which normally falls in the range of 5–13 $\times$ 10^{-6}/°C. This information is worthy consideration for the establishment of model codes for AASC in future.

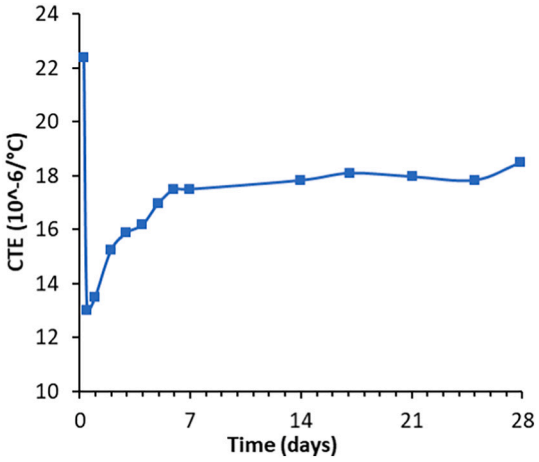

Fig. 12. CTE of AASC.

3.5. Elastic modulus of AASC under semi-adiabatic condition

The elastic modulus data measured by TSTM is shown in Fig. 13. It is seen that the concrete obtained a low elastic modulus (around 2 GPa) at 6 h. From 9 to 12 h, the elastic modulus increased sharply. This is consistent with the big increase of stress in this stage (Fig. 10). The increment of elastic modulus after 3d was minor. In early age, the elastic modulus values obtained during loading was slightly lower than that obtained during unloading. This is because non-plastic deformation could develop under compression, so not all deformation would recover

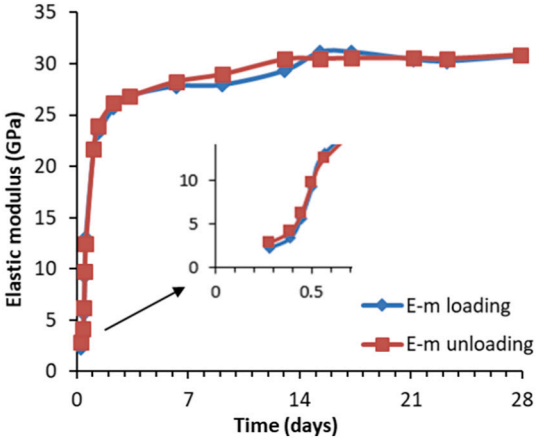

Fig. 13. Elastic modulus of AASC.

Fig. 11. Cracking (a) and the fracture surface (b) of the concrete.

during unloading. In longer curing age, the concrete became more and more stiff so the influence of non-elasticity became smaller. The elastic modulus results obtained by unloading will be used to model the stress evolution in the next section.

It should be noted that the stress generated in restrained AASC was mostly tensile stress, which should be correlated to tensile elastic modulus. In this study, however, the elastic modulus was measured only in compression, to avoid uncertainty in damage or non-elastic behaviour of the concrete under tensile force. We therefore have to assume that the elastic modulus of AASC under tension is identical to that under compression [43].

Compared with traditional methods to measure the elastic modulus of concrete by hydraulic compression testing machines [44,45], using TSTM can save lots of time in sample preparation and instalment when a series of data points is to be obtained. More importantly, using TSTM allows measurements from a very early age without the need to wait for demoulding. The EMM-ARM method proposed in [46] is another alternative for continuous measurement of elastic modulus since casting, but the advantage of TSTM is that it can supply various temperatures for the curing, therefore is recommendable for samples that require non-ambient curing. In addition, testing the elastic modulus by TSTM can also avoid drying of the sample. The drying induced microcracking was suspected as one reason of the decreasing elastic modulus of AASC after a certain age [44,47]. Of course, the locally restrained autogenous shrinkage by the aggregates can also lead to microcracking [31], but this phenomenon has not been reported to cause decreasing elastic modulus yet. As shown in Fig. 13, the elastic modulus of AASC did not decrease at least within 28d. This indicates that the decreasing elastic modulus reported in the literatures should be due to the drying-induced microcracking. To increase the confidence in using AASC, long-term elastic modulus should be monitored in future studies.

4. Simulation results and discussion

4.1. Free deformation of AASC under semi-adiabatic condition

Currently, there is no available model to simulate the deformation of AAMs under semi-adiabatic condition based on either microstructure parameters or empirical equations. In this study, the approach is to separately simulate the autogenous deformation and thermal deformation of the concrete. The total deformation ε_{tot} is considered as the sum of them, as shown in Eq. (6).

$$\varepsilon_{tot} = \varepsilon_{au} + \varepsilon_{th} \tag{6}$$

where ε_{au} and ε_{th} are the autogenous and thermal deformation of AASC, respectively.

The autogenous shrinkage of the concrete under semi-adiabatic condition is simulated by considering the autogenous shrinkage obtained under isothermal condition and equivalent ages in different conditions [39], as shown in Eq. (7). According to [48], the autogenous shrinkage of sodium hydroxide and sodium silicate activated slag and fly ash is mainly dependent on the reaction degree, irrespective of the curing temperature. This provides evidence of the validity of this approach. Arrhenius law was used to calculate the equivalent age, as shown in Eq. (8) [48].

$$\varepsilon_{au,semi}(t) = \varepsilon_{au,iso}(t_{eq}) \tag{7}$$

where $\varepsilon_{au,\ semi}$ and $\varepsilon_{au,\ iso}$is the autogenous shrinkage of AASC under semi-adiabatic condition and isothermal condition at 20 °C, respectively. The autogenous shrinkage under isothermal curing condition of AASC, $\varepsilon_{au,\ iso}$, was published in [25]. t_{eq} is the equivalent age. Since the temperature was measured every minute (see Section 2.3.1), the time step to calculate t_{eq} is 1 min.

$$t_{eq}(T) = \sum_{k=1}^{n} exp\left(-\frac{E_a}{R} \bullet \left(\frac{1}{T(\tau_k)} - \frac{1}{T_{ref}}\right)\right) \bullet d\tau \tag{8}$$

where $T(\tau_k)$ of each time step is taken from the temperature history of AASC obtained under semi-adiabatic condition, see Fig. 7; E_a is the apparent activation energy. According to previous studies [49,50], the value of E_a is taken as 57.6 KJ/mol. R is the universal gas constant, 8.314 J/(K·mol); T_{ref} is the reference temperature, 20 °C, i.e. 293 K, under which temperature the isothermal autogenous shrinkage of AASC was measured.

The thermal deformation of the concrete under semi-adiabatic condition is calculated by Eq. (9).

$$\varepsilon_{th}(t) = \sum_{k=1}^{n} \alpha_{CTE}(\tau_k) \bullet \Delta T(\tau_k) \tag{9}$$

where $\varepsilon_{th}(t)$ is the thermal deformation at time t; $\alpha_{CTE}(\tau_k)$ is the CTE at time τ_k; ΔT is the temperature change of the concrete in the time interval (see Fig. 7). Since the temperature of the concrete was measured frequently (every minute), the length of each time interval depends on the one used in measuring CTE (Fig. 12).

The simulated autogenous and thermal deformations and their sum are shown in Fig. 14 (a). The curves indicate that the concrete expands in the beginning due to the temperature rise. Afterwards, autogenous shrinkage developed rapidly. From 12 h, the total deformation turns into shrinkage despite of the development of thermal expansion. From 1 to 3d, the shrinkage of AASC is enhanced due to the thermal shrinkage. After 4d, the thermal deformation stabilized, as consistent with the stabilized temperature in this period (Fig. 7 (c)). From then on, the autogenous shrinkage plays the major role in the total deformation.

The comparison between the simulated and measured total deformation is shown in Fig. 14 (b). It can be seen that the simulated curve matches quite well with the measured one. In the first day, there is a small discrepancy between the two curves, as shown in the panel in Fig. 14 (b). This might result from the small number of data points obtained for some inputs in the very early age. For example, as shown in Fig. 12, the CTE of concrete changed significantly in the first 2d, but only 4 points were measured in this period. Within each time interval, the CTE was assumed as a constant, which can lead to simulation error in the thermal deformation. Besides, in the prediction of autogenous shrinkage (Eq. (8)), the apparent activation energy E_a was taken as 57.6 KJ/mol from the literature. On one hand, this value can vary with mixture design, hence, the E_a of the AASC studied here may be different. On the other hand, this value changes with the reaction degree [51]. Therefore, the assumption of E_a as constant can lead to error in simulating autogenous shrinkage. Last but not the least, the coupled effects of autogenous and thermal deformation, e.g., the influence of temperature variations on capillary tension, were not considered in the simulation (see Eq. (6)). Despite, the general agreement between the simulated and measured results indicates the validity of the simulation approach used in this study.

4.2. Stress of restrained AASC under semi-adiabatic condition

The stress evolution of restrained AASC is simulated based on the measured total deformation (Fig. 9) and elastic modulus (Fig. 13). Since AAS systems have been reported to show significant viscoelasticity [22,23,31], relaxation needs to be considered in calculating the stress in restrained AASC. The equations are shown below.

$$\sigma(t) = \sum_{k=1}^{n} \Delta\sigma_{relax}(\tau_k) = \sum_{k=1}^{n} \Delta\sigma_{elas}(\tau_k) \bullet \psi(\tau_k) \tag{10}$$

$$\Delta\sigma_{elas}(t) = \Delta\varepsilon_{tot}(t) \bullet E(t) \tag{11}$$

where $\sigma(t)$ is the simulated stress at time t; $\Delta\sigma_{elas}(t)$ is the incremental

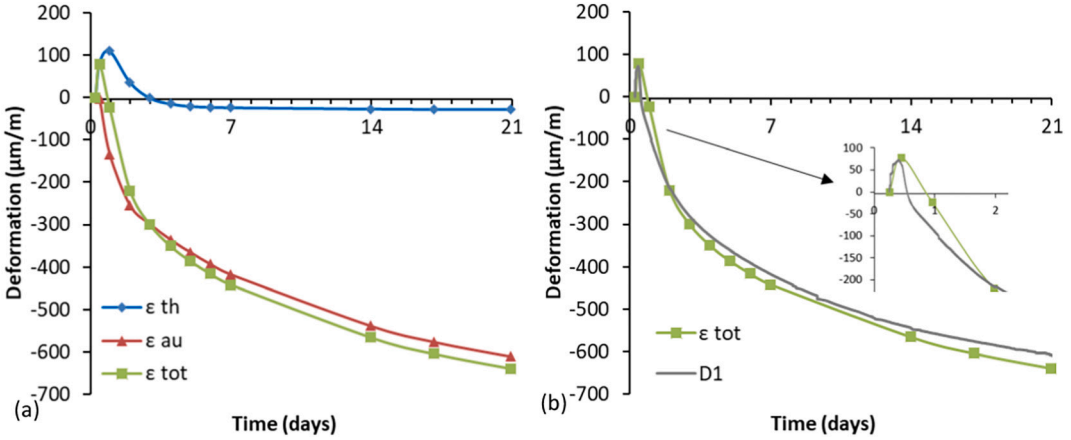

Fig. 14. Simulated autogenous, thermal and total deformations of AASC under semi-adiabatic condition (a). Comparison between the simulated and measured total deformation of AASC (b). The period of concern is 21d instead of 28d because of the lack of experimental data on autogenous shrinkage after 21d as reported in [25].

stress calculated from the increments of free deformation $\Delta\varepsilon_{tot}(t)$ and the elastic modulus $E(t)$; $\Delta\sigma_{relax}(\tau_k)$ is the simulated stress considering the relaxation; $\psi(\tau_k)$ is the relaxation factor, which can be calculated by Eq. (12) [25,52].

$$\psi(t,\tau) = e^{-\varphi(t,\tau)} \tag{12}$$

where φ is the creep coefficient at time t; τ is the time when the load is applied.

According to [25,52,53], the creep coefficient of OPC or AAMs based concrete can be calculated by Eq. (13).

$$\varphi(t,\tau) = \left(\frac{\alpha(t)}{\alpha(\tau)} - 1\right) + 1.34{*}\omega^{1.65}\tau^{-d}(t-\tau)^{n}\frac{\alpha(t)}{\alpha(\tau)} \tag{13}$$

where α is the degree of reaction; ω is the water-to-binder ratio (0.344, see Section 2.2); n is the relaxation factor whose value is empirically taken as 0.3 and d is the constant whose value is empirically taken as 0.35 according to [53].

The reaction degree α of the concrete can be calculated with Eq. (14) [54–56]. Equivalent age should be used when the reaction heat result was obtained under a different temperature history.

$$\alpha(t) = \frac{Q(t_{eq})}{Q_{max}} \tag{14}$$

where Q is the reaction heat and Q_{max} is the ultimate total heat at the completion of the reaction. $Q(t)$ and Q_{max} results of AASC under isothermal condition have been published in [23,25], hence not shown here.

With Eqs. (10)–(14), the stress in restrained AASC is calculated, as shown in Fig. 15. The evolution of σ_{elas} generally agrees with that of the measured stress, but the value is greatly overestimated in the whole period studied. With relaxation considered, σ_{relax} is much closer to the measured stress. Within 18 h, the compressive and tensile stresses are both overestimated by σ_{relax}. This is probably because the concrete shows pronounced viscoelasticity in the very early age, as confirmed by the dramatically high CTE in this period (Fig. 12). The relaxation factor in this stage may be larger than predicted by Eqs. (12)–(13), in which the same constants were used for concrete of all curing ages. Besides, the time interval (>2 h) in which the elastic modulus was measured determines the limited number of data points in this period. In each time interval, the parameters are assumed constants, while the real ones experience drastic changes. This brings extra error to the simulation. After 18 h, nonetheless, σ_{relax} matches nearly perfect with the measured stress. This indicates that the simulation approach proposed in this study is useful to predict the stress evolution in restrained AASC under semi-adiabatic condition. The results confirm that relaxation has to be considered in stress prediction, which is vital for the evaluation of the cracking potential of restrained concrete.

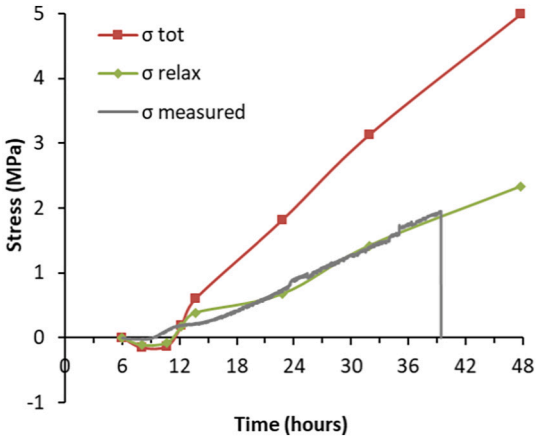

Fig. 15. Simulated stress of restrained AASC under semi-adiabatic condition. $\sigma_{measured}$ is the measured stress as shown in Fig. 10.

5. Additional remarks

This study provides experimental and numerical results on the deformation and stress of AASC under semi-adiabatic condition. All experiments were conducted under a same temperature history. This temperature history has practical implications in addition to the scientific value. For example, the concrete element used in a real project in the Netherlands [57] experienced similar temperature evolution (unpublished results). Of course, both the deformation and stress values will be different for other mixture designs or curing conditions. Although it is impossible for one study to cover all cases in practice, the experimental and numerical approaches provided in this study have the potential to be generalized for various mixtures and temperature histories. As confirmed in this study, the influence of temperature change on autogenous shrinkage of AASC can be estimated based on equivalent age calculated from Arrhenius law. Thermal deformation can be estimated based on the temperature history if the CTE is known. The total deformation, as a result, can be simulated as the sum of these two deformations. While it is known that relaxation has to be considered when predicting the stress, the way how relaxation factor can be obtained varies. In this study, the factor is calculated by equations involving empirical parameters from the literature. Future studies that can provide experimental data on early-age creep or relaxation of AAMs are surely

beneficial to validate relevant models.

6. Conclusions

In this study, thermal deformation and stress of AASC cured under semi-adiabatic condition were investigated by both experimental and simulation. The main conclusions of this study are summarised as below:

1. Cured under semi-adiabatic condition, the AASC (l/b = 0.5, binder content 400 kg/m^3) experienced a temperature increase of around 10 °C within 1 day and then cooling to around 20 °C in 4d. The temperature surge was less intensive than that of the OPC concrete (w/c = 0.5, binder content 350 kg/m^3) cured in the same mould.
2. The AASC showed expansion after casting due to temperature rise. However, the compressive stress generated by the initial expansion in restrained AASC was rather limited due to the low stiffness of the concrete. The thermal expansion was compensated by autogenous shrinkage soon even before the ending of acceleration period. The results reveal the twofold effects of temperature rise: on one hand it can induce thermal expansion, while on the other hand, it can enhance the autogenous shrinkage. The final deformation depends actually on the competition between these two deformations.
3. During cooling down, the concrete shrank sharply contributed by both thermal and autogenous shrinkages. The large shrinkage induced a high tensile stress in the restrained AASC and occurrence of cracking at around 40 h. The results indicate that semi-adiabatic condition is severer for AASC than isothermal condition in view of cracking tendency.
4. The CTE of AASC was higher than 20×10^{-6}/°C in the first hours and then decreased to 13×10^{-6}/°C as the stiffness grew. From 1d to 7d, the CTE increased gradually reaching around 18×10^{-6}/°C before stabilization. The measuring approach appears feasible to measure the CTE evolution of concrete under varying curing temperature.
5. The elastic modulus of AASC developed rapidly in the first 3d. Within 28d, no decrease in elastic modulus was observed. Using TSTM to measure the elastic modulus evolution of concrete has several advantages, including early starting time, lower labour intensity, and the possibility to apply various curing temperatures while avoiding drying.
6. Simulating the deformation of AASC under semi-adiabatic condition by the sum of thermal and autogenous deformations is proved feasible. Thermal deformation can be calculated from the temperature history and CET. Equivalent age needs to be used when the inputting autogenous shrinkage was obtained from a different curing condition.
7. Simply timing the semi-adiabatic deformation and elastic modulus will greatly overestimate the stress in restrained AASC. With the consideration of creep and relaxation, by contrast, the stress evolution can be predicted pretty well by the model used in this paper. This method can be useful for the estimation of cracking potential of restrained concrete.

CRediT authorship contribution statement

Zhenming Li: Conceptualization, Methodology, Investigation, Software, Writing-original draft, Writing – review & editing. **Xuhui Liang:** Investigation. **Chen Liu:** Investigation. **Minfei Liang:** Investigation, Data curation. **Klaas van Breugel:** Supervision, Writing – review & editing. **Guang Ye:** Supervision, Resources.

Declaration of competing interest

The authors declare that they have no known competing financial interests or personal relationships that could have appeared to influence the work reported in this paper.

Acknowledgment

The authors would like to thank the support from Microlab, Delft University of Technology.

Appendix A

The final setting time of the concrete measured by Vicat method was 35 min [44]. However, this does not mean the gain of a considerable stiffness by the concrete. The elastic modulus of the concrete remained low in the first hours. The elastic modulus of AAS paste measured by ambient response method is shown in Fig. A1 [23]. It can be seen the elastic modulus of AAS paste remains lower than 1 GPa in the first 6 h. Significant increase of elastic modulus did not occur at final setting time, but during the acceleration period (6–12 h [23]) of the reaction. The final setting time seems an indication of the loss of fluidity rather than of the formation of a stiff network [58]. This is also the reason why by traditional pressing method, the elastic modulus cannot be tested just after final setting. Of course, with the incorporation of aggregate, the stiffness evolution of AASC may not be identical to that of AAS paste shown in Fig. A1, but the difference should not be substantial. This point is verified in Section 3.5, which shows the elastic modulus of AASC reached only around 2 GPa at 6 h.

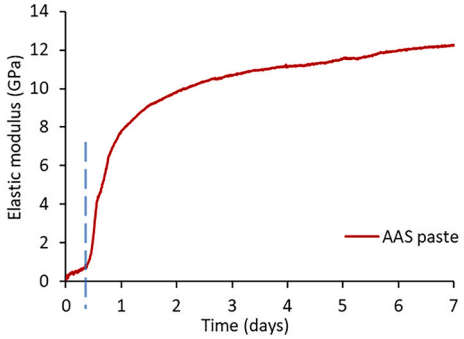

Fig. A1. Evolution of elastic modulus of AAS paste. The dashed line indicates the instants when the elastic modulus starts to rapidly increase.

References

[1] P. Duxson, J.L. Provis, G.C. Lukey, J.S.J. van Deventer, The role of inorganic polymer technology in the development of "green concrete", Cem. Concr. Res. 37 (2007) 1590–1597, https://doi.org/10.1016/j.cemconres.2007.08.018.

[2] J.L. Provis, J.S.J.Van Deventer, Geopolymers: Structures, Processing, Properties and Industrial Applications, Woodhead, Cambridge, UK, 2009.

[3] K. Arbi, M. Nedeljković, Y. Zuo, G. Ye, A review on the durability of alkali-activated Fly Ash/Slag systems: advances, issues, and perspectives, Ind. Eng. Chem. Res. 55 (2016) 5439–5453, https://doi.org/10.1021/acs.iecr.6b00559.

[4] G. Fang, W.K. Ho, W. Tu, M. Zhang, Workability and mechanical properties of alkali-activated fly ash-slag concrete cured at ambient temperature, Constr. Build. Mater. 172 (2018) 476–487.

[5] M.A. Longhi, Z. Zhang, B. Walkley, E.D. Rodríguez, A.P. Kirchheim, Strategies for control and mitigation of efflorescence in metakaolin-based geopolymers, Cem. Concr. Res. 144 (2021), 106431.

[6] M. Nedeljković, Z. Li, G. Ye, Setting, strength, and autogenous shrinkage of alkali-activated Fly ash and slag pastes: effect of slag content, Materials (Basel) 11 (2018) 2121, https://doi.org/10.3390/ma11112121.

[7] S. Wang, X. Pu, K.L. Scrivener, P.L. Pratt, Alkali-activated slag cement and concrete: a review of properties and problems, Adv. Cem. Res. 7 (1995) 93–102, https://doi.org/10.1680/adcr.1995.7.27.93.

[8] A.M. Neville, Properties of Concrete, Longman, London, 2011.

[9] O.M. Jensen, P.F. Hansen, Autogenous deformation and RH-change in perspective, Cem. Concr. Res. 31 (2001) 1859–1865, https://doi.org/10.1016/S0008-8846(01)00501-4.

[10] H. Ye, Mechanisms and Mitigation of Shrinkage in Alkali-activated Slag, The Pennsylvania State University, 2016.

[11] Z. Li, Autogenous Shrinkage of Alkali-activated Slag and Fly Ash Materials From Mechanism to Mitigating Strategies, Delft University of Technology, 2021.

[12] S. Uppalapati, Early-age Structural Development and Autogenous Shrinkage of Alkali-activated Slag/fly-ash Cements, KU Leuven, 2021.

[13] N.K. Lee, J.G. Jang, H.K. Lee, Shrinkage characteristics of alkali-activated fly ash/slag paste and mortar at early ages, Cem. Concr. Compos. 53 (2014) 239–248, https://doi.org/10.1016/j.cemconcomp.2014.07.007.

[14] W.R.L. da Silva, V. Šmilauer, P. Štemberk, Upscaling semi-adiabatic measurements for simulating temperature evolution of mass concrete structures, Mater. Struct. 48 (2015) 1031–1041.

[15] E.J. Bjøntegaard, Ø. Sellevold, Interaction between thermal dilation and autogenous deformation in high performance concrete, Mater. Struct. 34 (2001) 266–272.

[16] K. Orosz, A. Humad, H. Hedlund, A. Cwirzen, Autogenous deformation of alkali-activated blast furnace slag concrete subjected to variable curing temperatures, Adv. Civ. Eng. 2019 (2019) 1–8, https://doi.org/10.1155/2019/6903725.

[17] L. Zuda, R. Černý, Measurement of linear thermal expansion coefficient of alkali-activated aluminosilicate composites up to 1000 °C, Cem. Concr. Compos. 31 (2009) 263–267, https://doi.org/10.1016/j.cemconcomp.2009.02.002.

[18] F. Rifai, A. Darquennes, F. Benboudjema, B. Muzeau, L. Stefan, Study of shrinkage restraint effects at early-age in alkali-activated slag mortars, in: 9th Int. Conf. Fract. Mech. Concr. Concr. Struct., Berkeley, USA, 2016, https://doi.org/10.21012/fc9.240.

[19] J. Seo, S.J. Bae, D.I. Jang, S. Park, B. Yang, H.K. Lee, Thermal behavior of alkali-activated fly ash/slag with the addition of an aerogel as an aggregate replacement, Cem. Concr. Compos. 106 (2020), 103462, https://doi.org/10.1016/j.cemconcomp.2019.103462.

[20] M. Almakhadmeh, A.M. Soliman, Effects of mixing water temperatures on properties of one-part alkali-activated slag paste, Constr. Build. Mater. 266 (2021), 121030.

[21] L. Li, V. Dao, P. Lura, Autogenous deformation and coefficient of thermal expansion of early-age concrete: initial outcomes of a study using a newly-developed temperature stress testing machine, Cem. Concr. Compos. 119 (2021), 103997, https://doi.org/10.1016/j.cemconcomp.2021.103997.

[22] H. Ye, A. Radlińska, Shrinkage mechanisms of alkali-activated slag, Cem. Concr. Res. 88 (2016) 126–135, https://doi.org/10.1016/j.cemconres.2016.07.001.

[23] Z. Li, T. Lu, X. Liang, H. Dong, G. Ye, Mechanisms of autogenous shrinkage of alkali-activated slag and fly ash pastes, Cem. Concr. Res. 135 (2020), 106107, https://doi.org/10.1016/j.cemconres.2020.106107.

[24] S.J. Lokhorst, Deformational Behaviour of Concrete Influenced by Hydration Related Changes of the Microstructure, Delft University of Technology, 2001.

[25] Z. Li, S. Zhang, X. Liang, G. Ye, Cracking potential of alkali-activated slag and fly ash concrete subjected to restrained autogenous shrinkage, Cem. Concr. Compos. 114 (2020), 103767, https://doi.org/10.1016/j.cemconcomp.2020.103767.

[26] M. Irfan-Ul-Hassan, B. Pichler, R. Reihsner, C. Hellmich, Elastic and creep properties of young cement paste, as determined from hourly repeated minute-long quasi-static tests, Cem. Concr. Res. 82 (2016) 36–49, https://doi.org/10.1016/j.cemconres.2015.11.007.

[27] B. Delsaute, C. Boulay, J. Granja, J. Carette, M. Azenha, C. Dumoulin, G. Karaiskos, A. Deraemaeker, S. Staquet, Testing concrete E-modulus at very early ages through several techniques: an inter-laboratory comparison, Strain (2016) 91–109, https://doi.org/10.1111/str.12172.

[28] Z. Li, M. Nedeljković, B. Chen, G. Ye, Mitigating the autogenous shrinkage of alkali-activated slag by metakaolin, Cem. Concr. Res. 122 (2019) 30–41, https://doi.org/10.1016/j.cemconres.2019.04.016.

[29] C. Shi, D. Roy, P. Krivenko, Alkali-activated Cements and Concretes, CRC press, 2003.

[30] L. Liu, J. Ouyang, F. Li, J. Xin, D. Huang, S. Gao, Research on the crack risk of early-age concrete under the temperature stress test machine, Materials (Basel) 11 (2018) 1822.

[31] Z. Li, T. Lu, Y. Chen, B. Wu, G. Ye, Prediction of the autogenous shrinkage and microcracking of alkali-activated slag and fly ash concrete, Cem. Concr. Compos. 117 (2021), https://doi.org/10.1016/j.cemconcomp.2020.103913.

[32] Z. Li, M. Wyrzykowski, H. Dong, J. Granja, M. Azenha, P. Lura, G. Ye, Internal curing by superabsorbent polymers in alkali-activated slag, Cem. Concr. Res. 135 (2020), 106123, https://doi.org/10.1016/j.cemconres.2020.106123.

[33] T. Zhang, W. Qin, Tensile creep due to restraining stresses in high-strength concrete at early ages, Cem. Concr. Res. 36 (2006) 584–591.

[34] E.J. Sellevold, Ø. Bjøntegaard, Coefficient of thermal expansion of cement paste and concrete: mechanisms of moisture interaction, Mater. Struct. 39 (2006) 809–815.

[35] H. Dettling, The thermal expansion of hardened cement paste, in: Aggregates, and Concrete, Bulletin, 1964.

[36] Y. Yang, R. Sato, A new approach for evaluation of autogenous shrinkage of high strength concrete under heat of hydration, in: Self-Desiccation Its Importance Concr. Technol, 2002, p. 1415.

[37] I. Maruyama, A. Teramoto, Impact of time-dependant thermal expansion coefficient on the early-age volume changes in cement pastes, Cem. Concr. Res. 41 (2011) 380–391, https://doi.org/10.1016/j.cemconres.2011.01.003.

[38] R. Loser, B. Münch, P. Lura, A volumetric technique for measuring the coefficient of thermal expansion of hardening cement paste and mortar, Cem. Concr. Res. 40 (2010) 1138–1147, https://doi.org/10.1016/j.cemconres.2010.03.021.

[39] P. Turcry, A. Loukili, L. Barcelo, J.M. Casabonne, Can the maturity concept be used to separate the autogenous shrinkage and thermal deformation of a cement paste at early age? Cem. Concr. Res. 32 (2002) 1443–1450, https://doi.org/10.1016/S0008-8846(02)00800-1.

[40] J. Carette, S. Joseph, Ö. Cizer, S. Staquet, Decoupling the autogenous swelling from the self-desiccation deformation in early age concrete with mineral additions : micro-macro observations and unified modelling, Cem. Concr. Compos. 85 (2018) 122–132.

[41] J. Mallela, A. Abbas, T. Harman, C. Rao, R. Liu, M.I. Darter, Measurement and significance of the coefficient of thermal expansion of concrete in rigid pavement design, Transp. Res. Rec. 1919 (2005) 38–46.

[42] T.R. Naik, R.N. Kraus, R. Kumar, Influence of types of coarse aggregates on the coefficient of thermal expansion of concrete, J. Mater. Civ. Eng. 23 (2011) 467–472.

[43] J.J. Brooks, A.M. Neville, A comparison of creep, elasticity and strength of concrete in tension and in compression, Mag. Concr. Res. 29 (1977) 131–141.

[44] Z. Li, B. Delsaute, T. Lu, A. Kostiuchenko, S. Staquet, G. Ye, A comparative study on the mechanical properties and autogenous shrinkage induced stress of alkali-activated concrete and ordinary Portland cement concrete, Constr. Build. Mater. 292 (2021), 123418, https://doi.org/10.1016/j.conbuildmat.2021.123418.

[45] NEN-EN 12390-13, Testing Hardened Concrete - Part 13: Determination of Secant Modulus of Elasticity in Compression, 2013.

[46] M. Azenha, F. Magalhães, R. Faria, Á. Cunha, Measurement of concrete E-modulus evolution since casting: a novel method based on ambient vibration, Cem. Concr. Res. 40 (2010) 1096–1105, https://doi.org/10.1016/j.cemconres.2010.02.014.

[47] S. Prinsse, D.A. Hordijk, G. Ye, P. Lagendijk, M. Luković, Time-dependent material properties and reinforced beams behavior of two alkali-activated types of concrete, Struct. Concr. 21 (2020) 642–658, https://doi.org/10.1002/suco.201900235.

[48] B. Delsaute, J. Gambacorta, S. Staquet, Influence of the Ms-modulus on the early-age volume change and heat release of slag and fly ash pastes activated by sodium hydroxide and sodium silicate, in: 4th Int. RILEM Conf. Microstruct. Relat. Durab. Cem. Compos, 2020, pp. 781–787.

[49] A. Fernández-Jiménez, F. Puertas, Alkali-activated slag cements: kinetic studies, Cem. Concr. Res. 27 (1997) 359–368, https://doi.org/10.1016/S0008-8846(97)00040-9.

[50] S. Zhang, Y. Zuo, Z. Li, G. Ye, Isothermal calorimetric study on heat evolution and apparent activation energy of alkali-activated slag/fly ash paste, in: 2nd Int. Conf. Sustain. Build. Mater., Eindhoven, 2019, pp. 1–8.

[51] J. Carette, S. Staquet, Monitoring and modelling the early age and hardening behaviour of eco-concrete through continuous non-destructive measurements: part I. Hydration and apparent activation energy, Cem. Concr. Compos. 73 (2016) 10–18, https://doi.org/10.1016/j.cemconcomp.2016.07.002.

[52] K.Van Breugel, in: Relaxation of Young Concrete, 1980, p. 144.

[53] H. van der Ham, E. Koenders, K. van Breugel, Creep model uncertainties in early-age concrete simulations, Proc. Concreep. 8 (2008) 431–436.

[54] K.A. Riding, J.L. Poole, K.J. Folliard, M.C.G. Juenger, A.K. Schindler, Modeling hydration of cementitious systems, ACI Mater. J. 109 (2012) 225–234.

[55] A.K. Schindler, K.J. Folliard, Heat of hydration models for cementitious materials, ACI Mater. J. 102 (2005) 24.

[56] D. Ravikumar, N. Neithalath, Reaction kinetics in sodium silicate powder and liquid activated slag binders evaluated using isothermal calorimetry, Thermochim. Acta 546 (2012) 32–43, https://doi.org/10.1016/j.tca.2012.07.010.

[57] E. Beerda, In Friesland durven ze het aan: een autobrug van beton zonder een gram cement, Cobouw, Oct 26, https://www.cobouw.nl/duurzaamheid/nieuws/2021/10/in-friesland-durven-ze-het-aan-een-autobrugdek-van-beton-zonder-cement-101299832#.YXkNZH91I1M.linkedin, 2021.

[58] M. Palacios, S. Gismera, M.M. Alonso, J.B. d'Espinose de Lacaillerie, B. Lothenbach, A. Favier, C. Brumaud, F. Puertas, Early reactivity of sodium silicate-activated slag pastes and its impact on rheological properties, Cem. Concr. Res. 140 (2021), 106302, https://doi.org/10.1016/j.cemconres.2020.106302.